MHD FLOW AND HEAT TRANSFER OF A TERNARY HYBRID FERROFLUID OVER A STRETCHING/SHRINKING POROUS SHEET WITH THE EFFECTS OF BROWNIAN DIFFUSION AND THERMOPHORESIS[†]

Michael I. Kopp[a]*, Volodymyr V. Yanovsky[a,b], Thippeswamy Anusha[c], Ulavathi S. Mahabaleshwar[c]

[a]Institute for Single Cristals, Nat. Academy of Science Ukraine, Nauky Ave. 60, Kharkiv 31001,Ukraine
[b]V.N. Karazin Kharkiv National University, 4, Svoboda Sq., Kharkiv, 61022, Ukraine
[c]Department of Mathematics, Shivagangotri, Davangere University, Davangere, India 577 007
*E-mail: michaelkopp0165@gmail.com
Received December 9, 2022; revised December 30, 2022; accepted December 31, 2022

In this paper, the magnetohydrodynamic (MHD) flow of a ternary hybrid ferrofluid over a stretching/shrinking porous sheet in the presence of radiation and mass transpiration is studied. The ternary hybrid ferrofluid is formed by suspending three types of nanoparticles for enhancing heat transfer. The nanoparticles of copper (Cu), iron oxide (Fe_3O_4), and cobalt ferrite ($CoFe_2O_4$) are suspended in water in this study, producing in the combination $Cu - Fe_3O_4 - CoFe_2O_4 - H_2O$. Brownian motion and thermophoresis are integrated into the ternary hybrid ferrofluid model. Similarity transformations convert the governing partial differential equations into ordinary differential equations. The boundary value problem (*bvp*) is used in the Maple computer software to solve transformed equations numerically. The computed results for relevant parameters such as velocity profile, temperature profile, skin friction coefficient, local Nusselt and Sherwood numbers are visually shown and explained in detail.

Keywords: *ternary hybrid ferrofluid; stretching/shrinking; heat and mass transfer; mass transpiration; magnetic field*
PACS: 44.10.+i, 44.30.+v, 44.05.+e

1. INTRODUCTION

For several decades, interest in studying the flow and heat transfer of the boundary layer on a stretching/shrinking sheet has not waned due to a wide range of technical applications such as medical, industrial, and mechanical engineering applications. Maxwell [1] was the first to try to improve the heat transfer rate of ordinary fluids by suspending micro-sized particles, but his experiment failed due to sedimentation and blocking of the flow patterns. Choi [2], Sakiadis [3]-[4], and Crane [5] initially researched nanofluids and stretching sheets. Following this, many researchers were interested in the topic and performed significant research in it. Nanofluids have a greater thermal conductivity than regular fluids, which is needed for the efficient transfer of thermal energy. According to studies, the thermal conductivity coefficient of nanofluids rises dramatically when compared to ordinary base fluids, even at extremely low nanoparticle concentrations [2]. Existing refrigerants in several industries, including energy, electronics, transportation, and manufacturing, can be replaced by nanofluids. In relation to this, researchers have been very interested in the applications of nanofluid since the discovery of this innovative idea.

Recently, a new type of nanofluid known as hybrid nanofluid has been created, which is formed by the suspension of several nanoparticles in the base fluid. MHD flow of hybrid nanofluid and heat transfer over a stretching/shrinking sheet was introduced by Aly and Pop [6]. Khan et al. [7] and Jamaludin et al. [8] examined hybrid nanofluids in different flow scenarios. Mahabaleshwar et al. [9] developed a hybrid nanofluid algebraically decaying approach. Mahabaleshwar et al. recently researched couple stress hybrid nanofluid [10], MHD flow micro polar fluid [11], and an MHD nanofluid through a penetrable and also stretching/shrinking surface, a horizontal surface with a radiated effect, and mass transpiration [12]. Heat transmission is enhanced by increasing the volume fraction of nanoparticles, according to the researchers.

Among the various hybrid nanofluids, we focus on hybrid ferrofluids. The study of ferrofluids is of great interest due to its wide application in biomedicine and technology, namely for drug delivery, real-time chemical monitoring of human brain activity, destruction of tumors, etc. Ferrofluids are colloidal liquids made of magnetic nanoparticles like cobalt ferrite $CoFe_2O_4$, hematite Fe_2O_3, magnetite Fe_3O_4, and many other nanometersized particles containing iron in the base fluid [13].

Chu et al. [14] investigated the thermal performance and flow properties of a hybridized nanofluid (*MWCNT* - Fe_3O_2 -water) in a cavity. Kumar et al. [15] studied the flow characteristics of hybrid ferrofluids (Fe_3O_4 - $CoFe_2O_4$) using water-ethylene glycol combination (50 % -50 %) as a basis fluid in thin film flow and found that hybrid ferrofluid enhances rate of heat transfer than ferrofluid. Tlili et al. [16] studied the stream and energy transport in magnetohydrodynamic dissipative ferro and hybrid ferrofluids by considering an uneven heat rise/fall and radiation

effects. They found that the magnetic oxide and cobalt iron oxide suspended in H_2O-EG (ethylene glycol) (50%-50%) mixture effectively reduces the heat transfer rate under specific conditions. Anuar et al. [17] investigated MHD hybrid ferrofluid flow on exponentially stretching/shrinking surfaces with heat source/sink effects under stagnation point region. They found that hybrid ferrofluid increases the rate of heat transfer compared to ferrofluid and for a stronger heat source, heat absorption is more likely to occur in the sheet. The effects of MHD and viscous dissipation have been studied by Lund et al, [18] considering ($Cu - Fe_3O_4 - H_2O$) hybrid nanofluid in a porous medium.

In recent years, a new class of nanofluids has emerged, consisting of three solid nanoparticles distributed in an ordinary liquid. The term ternary hybrid nanofluid is commonly used to describe these liquids [19]. Khan and Mahmood [20] presented a study of MHD ternary hybrid nanofluid flow into a stretching/shrinking cylinder with mass suction and either Joule heating. The combination of copper nanoparticles (Cu), iron oxide (Fe_3O_4), and silicon dioxide (SiO_2) with polymer as the base fluid has been chosen as an example of a ternary hybrid nanofluid. They showed that the heat transfer rate could be increased. Ramesh et al. [21] studied the increase of heat transfer in ternary nanofluid flows caused by stretched convergent or divergent channels. Temperature was reduced when the solid volume-fraction of both stretched and shrunk channels increased. It has also been found that ternary nanofluids have a stronger influence than hybrid and mono-nanofluids. Animasaun et al. [22] investigated the dynamics of stagnant ternary-hybrid nanofluid (i. e. water conveying spherical silver nanoparticles, cylindrical aluminum oxide nanoparticles, and platelet aluminum nanoparticles) when induced magnetic field and convective heating surface are significant. In [22], it was concluded that the increase in convective heating of the wall is a factor that can accelerate temperature dispersion in both the case of a heat source and a heat sink. It was shown that the growing effects of an inclined magnetic field can cause the distance between the shear stress turning points and the gradient of magnetic flux density to be placed near the domain's centre. Manjunatha et al. [23] presented a new theoretical ternary nanofluid model for enhancing heat transfer. The ternary hybrid nanofluid was formed by suspending the nanoparticles TiO_2, Al_2O_3, and SiO_2 in water thus forming the combination $TiO_2 - SiO_2 - Al_2O_3 - H_2O$. They showed that the ternary nanofluid flowing past a stretching sheet has better thermal conductivity than the hybrid nanofluid.

In the current study, we propose a new kind of ternary hybrid ferrofluid formed by suspending metallic nanoparticles of copper (Cu), iron oxide (Fe_3O_4), and cobalt ferrite ($CoFe_2O_4$) in water (H_2O). Copper nanoparticles have rather high values of thermal and electrical conductivity coefficients; therefore, their use in ternary hybrid ferrofluids will enhance heat transfer, which is very important for solving some medical problems.

The purpose of the present investigation is to study the boundary layer flow and heat transfer past a stretching/shrinking sheet in a porous medium saturated by a ternary hybrid ferrofluid. The governing partial differential equations are transformed into a set of ordinary differential equations using a similarity transformation, before being solved numerically by the *bvp* method. The results obtained are presented graphically and discussed. This theoretical study will be useful to engineers conducting experiments with ternary hybrid ferrofluid.

2. STATEMENT OF THE PROBLEM AND MATHEMATICAL MODEL

We consider the two-dimensional steady flow and heat transfer of MHD ternary hybrid ferrofluid past a permeable stretching/shrinking sheet of a porous medium. The x-axis is chosen to run parallel to the horizontal surface, whereas the y-axis is chosen to run perpendicular to it. The surface velocity is assumed to be $u_w(x)$, and the mass flux velocity is v_0, with $v_0 < 0$ for suction and $v_0 > 0$ for fluid injection. The applied magnetic field B_0 is determined along the sheet's normal. It is also assumed that the constant temperature and constant nanofluid volume fraction of the sheet's surface are T_w and C_w, respectively, whereas the ambient fluid's are T_∞ and C_∞. This physical model is shown in Fig.1.
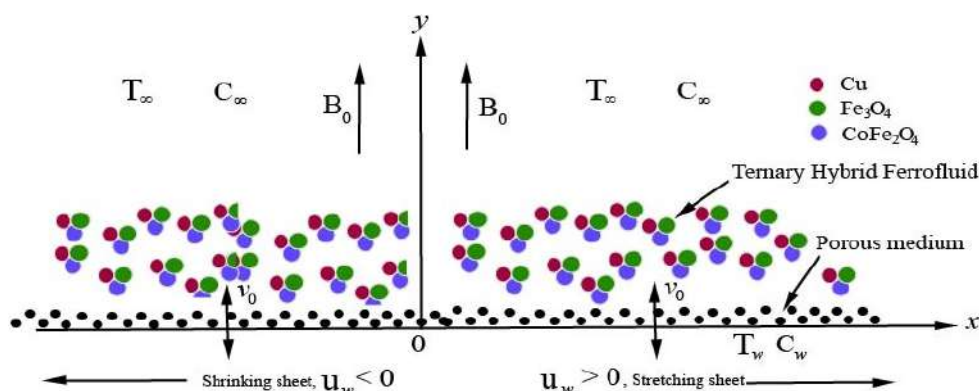

Figure 1. Coordinate system and physical model: stretching and shrinking shee.

The investigating physical model's basic equations can be written as

$$\frac{\partial u}{\partial x} + \frac{\partial v}{\partial y} = 0 \tag{1}$$

$$u\frac{\partial u}{\partial x} + v\frac{\partial u}{\partial y} = \frac{\mu_{thf}}{\rho_{thf}}\frac{\partial^2 u}{\partial y^2} - \frac{\mu_{thf}}{K\rho_{thf}}u - \frac{\sigma_{thf}}{\rho_{thf}}B_0^2 u \tag{2}$$

$$u\frac{\partial T}{\partial x} + v\frac{\partial T}{\partial y} = \frac{k_{thf}}{(\rho C_p)_{thf}}\frac{\partial^2 T}{\partial y^2} + \tag{3}$$

$$+\delta\left[D_B\frac{\partial C}{\partial y}\frac{\partial T}{\partial y} + \frac{D_T}{T_\infty}\left(\frac{\partial T}{\partial y}\right)^2\right] - \frac{1}{(\rho C_p)_{thf}}\frac{\partial q_r}{\partial y}$$

$$u\frac{\partial C}{\partial x} + v\frac{\partial C}{\partial y} = D_B\frac{\partial^2 C}{\partial y^2} + \frac{D_T}{T_\infty}\frac{\partial^2 T}{\partial y^2} \tag{4}$$

The following are the boundary conditions for the investigated model:

$$u = u_w = U_w(x)\lambda, \ v = v_0, \ T = T_w, \ C = C_w, \text{ at } y = 0 \tag{5}$$

$$u \to 0, \ T = T_\infty, \ C = C_\infty, \text{ at } y \to \infty \tag{6}$$

Here K is the permeability of a porous medium, T denotes the temperature of the ternary hybrid nanofluid, C the concentration of nanoparticles, D_B the Brownian diffusion coefficient, D_T the thermophoretic diffusion coefficient, and $\delta = (\rho C_p)_s / (\rho C_p)_f$ the ratio of nanoparticle heat capacity to base fluid heat capacity. Further, μ_{thf} is the dynamic viscosity of the ternary hybrid nanofluids, ρ_{thf} is the density of the ternary hybrid nanofluids, and k_{thf} is the ternary hybrid nanofluid's thermal conductivity, σ_{thf} the electrical conductivity, $(\rho C_p)_{thf}$ is the ternary hybrid nanofluid's heat capacity, λ is the constant stretching/shrinking parameter, with $\lambda > 0$ for a stretching sheet, $\lambda < 0$ for a shrinking sheet, and $\lambda = 0$ for a static sheet. Furthermore, we assume that $U_w(x) = ax$, where a is a positive constant.

In this study, the physical quantities of interest are the local skin friction coefficient C_{fx}, the local Nusselt number Nu_x, and the local Sherwood number Sh_x, which are defined as follows [24]:

$$C_{fx} = \frac{\mu_{thf}}{\rho_f a^2 x^2}\left(\frac{\partial u}{\partial y}\right)_{y=0},$$

$$Nu_x = -\frac{xk_{thf}}{k_f(T_w - T_\infty)}\left(\frac{\partial T}{\partial y}\right)_{y=0}, \tag{7}$$

$$Sh_x = -\frac{D_B x}{D_B(C_w - C_\infty)}\left(\frac{\partial C}{\partial y}\right)_{y=0}.$$

Let the ternary hybrid ferrofluid be composed of three sorts of nanoparticles, denoted by indices 1, 2, and 3. The nanofluid is formed by first adding copper nanoparticles (Cu) to water-based base fluid. Then a hybrid nanofluid is prepared by adding iron oxide (Fe_3O_4) nanoparticles to the nanofluid. Finally, a ternary hybrid nanofluid is formed by adding cobalt iron oxide ($CoFe_2O_4$) nanoparticles to the hybrid nanofluid. The overall volume fraction is the summation of the volume concentration of two dissimilar kinds of nanoparticles: $\phi = \phi_1 + \phi_2 + \phi_3$.

The thermophysical properties of the $Cu - H_2O$ nanofluid have been studied in many works. For example, Raza et al. [25] obtained several solutions for the rheology of the $Cu - H_2O$ nanofluid in a porous heat transfer channel. Lund et al. [18] identified the thermophysical properties of hybrid ferrofluid ($Fe_3O_4 - CoFe_2O_4 - H_2O$). Takabi and

Salehi [26], Gorla et al. [27], and Anuar et al. [17] describe the thermophysical properties of hybrid ferrofluid $(Fe_3O_4 - CoFe_2O_4 - H_2O)$. The thermophysical properties of $Cu - Fe_3O_4 - CoFe_2O_4 - H_2O$ ternary hybrid nanofluid are

• Density

$$\rho_{thf} = (1-\phi_3)\left\{(1-\phi_2)[(1-\phi_1)\rho_f + \phi_1\rho_{s1}] + \phi_2\rho_{s2}\right\} + \phi_3\rho_{s3} \qquad (8)$$

• Thermal conductivity

$$\frac{k_{thf}}{k_{hnf}} = \frac{k_{s3} + 2k_{hnf} - 2\phi_3(k_{hnf} - k_{s3})}{k_{s3} + 2k_{hnf} + \phi_3(k_{hnf} - k_{s3})}, \text{ where} \qquad (9)$$

$$\frac{k_{hnf}}{k_{nf}} = \frac{k_{s2} + 2k_{nf} - 2\phi_2(k_{nf} - k_{s2})}{k_{s2} + 2k_{nf} + \phi_2(k_{nf} - k_{s2})}, \text{ and}$$

$$\frac{k_{nf}}{k_f} = \frac{k_{s1} + 2k_f - 2\phi_1(k_f - k_{s1})}{k_{s1} + 2k_f + \phi_1(k_f - k_{s1})}.$$

• Heat capacity

$$(\rho C_p)_{thf} = (1-\phi_3)\left\{(1-\phi_2)[(1-\phi_1)(\rho C_p)_f + \phi_1(\rho C_p)_{s1}] + \phi_2(\rho C_p)_{s2}\right\} + \phi_3(\rho C_p)_{s3} \qquad (10)$$

• Dynamic viscosity

$$\frac{\mu_{thf}}{\mu_f} = \frac{1}{(1-\phi_1)^{2.5}(1-\phi_2)^{2.5}(1-\phi_3)^{2.5}} \qquad (11)$$

• Electrical conductivity

$$\frac{\sigma_{thf}}{\sigma_{hf}} = \frac{(1+2\phi_3)\sigma_{s3} + (1-2\phi_3)\sigma_{hnf}}{(1-\phi_3)\sigma_{s3} + (1+\phi_3)\sigma_{hnf}}, \text{ where} \qquad (12)$$

$$\frac{\sigma_{hnf}}{\sigma_{nf}} = \frac{(1+2\phi_2)\sigma_{s2} + (1-2\phi_2)\sigma_{nf}}{(1-\phi_2)\sigma_{s2} + (1+\phi_2)\sigma_{nf}}, \text{ and}$$

$$\frac{\sigma_{nf}}{\sigma_f} = \frac{(1+2\phi_1)\sigma_{s1} + (1-2\phi_1)\sigma_f}{(1-\phi_1)\sigma_{s1} + (1+\phi_1)\sigma_f}.$$

Here, ρ_f is the density of the base fluid, σ_f, k_f is the electrical and thermal conductivity of the base fluid. $(\rho C_p)_f$ is the heat capacity of the base fluid, and C_p is the heat capacity at the constant pressure of the base fluid. The subscripts $s1, s2$, and $s3$ denote the characteristics of nanoparticles Cu, Fe_3O_4, and $CoFe_2O_4$, respectively. Table 1 shows the thermophysical constants for nanoparticles and base fluid.

Table1. Thermophysical properties of the nanoparticles and base fluid [18],[27]

	$\rho[kg \cdot m^{-3}]$	$C_p[J \cdot kg^{-1} \cdot K^{-1}]$	$k[W \cdot m^{-1} \cdot K^{-1}]$	$\sigma[S \cdot m^{-1}]$
H_2O	997.1	4179	0.613	0.05
Cu	8933	385	401	$5.96 \cdot 10^7$
Fe_3O_4	5180	670	9.7	$7.4 \cdot 10^5$
$CoFe_2O_4$	4907	700	3.7	$1.1 \cdot 10^7$

3. SIMILARITY TRANSFORMATION AND PHYSICAL QUANTITIES

The partial differential equations (1)-(4) are transformed into ordinary differential equations through similarity transformation (see, for example, [28]):

$$u = \frac{x\nu_f}{L^2}\frac{\partial f(\eta)}{\partial \eta}, v = -\frac{\nu_f}{L}f(\eta), \eta = \frac{y}{L}, \theta(\eta) = \frac{T-T_\infty}{T_w - T_\infty}, \varphi(\eta) = \frac{C-C_\infty}{C_w - C_\infty}, \qquad (13)$$

where v_f is the kinematic viscosity of the base fluid, f, θ, φ are the dimensionless functions. L is a reference length that will be found further below. Furthermore, the radiant heat flow q_r is given by using the Rosseland approximation for radiation (see [29]):

$$\frac{1}{(\rho C_p)_{hf}}\frac{\partial q_r}{\partial y} \approx -\frac{16\kappa T_\infty^3}{3(\rho C_p)_{hf} k^*}\frac{\partial T}{\partial y} \tag{14}$$

where σ^*, k^* is the Stefan-Boltzmann constant and the mean absorption coefficient, respectively. It is interesting to note that, according to the definitions of u and v, equation (1) is automatically satisfied. Equations (2)-(4), as well as the boundary conditions (5)-(6), are transformed into the ordinary (similarity) differential equations shown below:

$$A_1 f''' + ff'' - f'^2 - (A_2 + A_3 \cdot M)f' = 0 \tag{15}$$

$$A_4 \theta'' + N_B \varphi' \theta' + N_T \theta'^2 + f\theta' = 0 \tag{16}$$

$$\varphi'' + Lef\varphi' + \frac{N_T}{N_B}\theta'' = 0 \tag{17}$$

$$f(0) = s, f'(0) = \lambda, \theta(0) = 1, \varphi(0) = 1, \text{ at } \eta = 0 \tag{18}$$

$$f''(\eta) \to 0, \theta(\eta) \to 0, \varphi(\eta) \to 0, \text{ at } \eta \to \infty \tag{19}$$

Primes denote differentiation with regard to η in this context. Using the boundary conditions (18)-(19), we find expressions for L and v_0

$$L = \sqrt{\frac{v_f}{a}}, v_0 = -\sqrt{av_f}\, s \tag{20}$$

The following ratios are used in Equations (15)-(16):

$$A_1 = \frac{\mu_{thf}/\mu_f}{\rho_{thf}/\rho_f}, A_2 = A_1 \cdot \frac{v_f}{aK}, A_3 = \frac{\sigma_{thf}/\sigma_f}{\rho_{thf}/\rho_f}, \tag{21}$$

$$A_4 = \frac{1}{Pr} \cdot \frac{k_{thf}/k_f}{(\rho C_p)_{thf}/(\rho C_p)_f} + \frac{(\rho C_p)_f}{(\rho C_p)_{thf}} \cdot \frac{Nr}{Pr}. \tag{}$$

Where M, Pr, Nr, Le, N_B and N_T denote the magnetic parameter, Prandtl number, radiation parameter, Lewis number, Brownian motion parameter and thermophoresis parameter, respectively, where

$$M = \frac{B_0^2 \sigma_f}{a\rho_f}, Pr = \frac{v_f(\rho C_p)_f}{k_f}, Nr = \frac{16\sigma^* T_\infty^3}{3k_f k^*}, Le = \frac{v_f}{D_B}, \tag{22}$$

$$N_B = \frac{\delta D_B(C_w - C_\infty)}{v_f}, N_T = \frac{\delta D_T(T_w - T_\infty)}{v_f T_\infty}. \tag{}$$

Using the similarity variables (13), one can easily obtain the expressions for physical quantities (7):

$$C_{fx}\sqrt{Re_x} = \frac{\mu_{thf}}{\mu_f}f''(0), Nu_x(\sqrt{Re_x})^{-1} = -\frac{k_{thf}}{k_f}\theta'(0), \tag{23}$$

$$Sh_x(\sqrt{Re_x})^{-1} = -\varphi'(0),$$

where $Re_x = U_w x / v_f$ is the local Reynolds number.

4. MODIFIED SYSTEM OF EQUATIONS

The exact analytical solution to the equation for the dimensionless stream function is represented as (see, for example, [5])

$$f(\eta) = \alpha_1 + \alpha_2 \exp(-\beta\eta) \tag{24}$$

Applying boundary conditions (18) to the solution (24), we find expressions for the constants α_1 and α_2. As a result, solution (24) takes the following form

$$f(\eta) = s + \frac{\lambda}{\beta}(1 - \exp(-\beta\eta)) \tag{25}$$

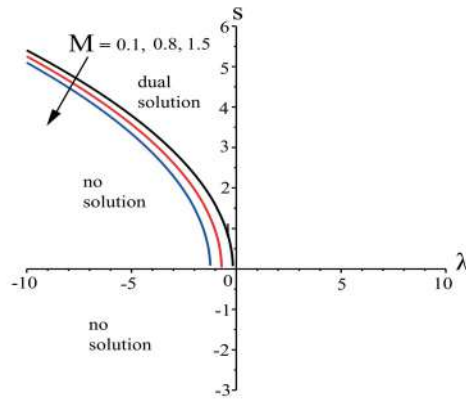Clearly, β may be found by substituting the relation (25) in Eq. (15):

Figure 2. Regions of solutions of s as a function of λ for stretching/shrinking sheet when $\phi_1 = 0.1$, $\phi_2 = 0.01$ and $\phi_3 = 0.02$.
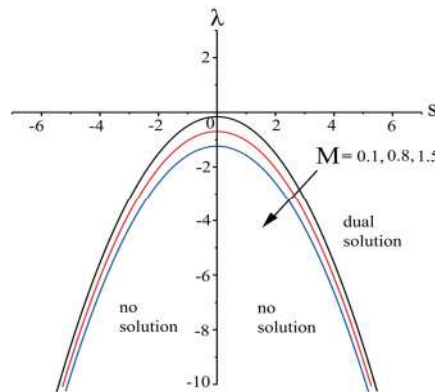

Figure 3. Regions of solutions of λ as a function of s for stretching/shrinking sheet when $\phi_1 = 0.1$, $\phi_2 = 0.01$ and $\phi_3 = 0.02$.

$$\beta = \frac{s}{2A_1} \pm \sqrt{\frac{s^2}{4A_1^2} + \frac{A_2 + A_3 \cdot M + \lambda}{A_1}} \tag{26}$$

It's obvious that physical solution correspond to a positive value of β, when $\lambda > 0$ (stretched sheet) for any value of s. Fig. 2 depicts the influence of the external magnetic field on the region of no, unique and dual solutions s depending on λ for a stretching/shrinking sheet. With an increase in the magnetic field, the curve of critical values s shifts towards negative parameters λ. Similarly, in Fig. 3, curves are plotted for the critical λ depending on the magnitude of the magnetic field. We see that as the magnetic field increases, the regions of no, unique, and dual solutions shift towards negative λ.

After calculating β, we find an analytical solution for $f(\eta)$ (25). Then the skin friction coefficient (Sr) is given by:

$$Sr = C_{fx}\sqrt{Re_x} = \frac{\mu_{thf}}{\mu_f}\lambda\beta \tag{27}$$

By substituting this solution into equations (16)-(17), we obtain the modified system of equations shown below:

$$A_4\theta'' + N_B\varphi'\theta' + N_T\theta'^2 + \left(s + \frac{\lambda}{\beta}(1 - \exp(-\beta\eta))\right)\theta' = 0 \tag{28}$$

$$\varphi'' + Le\left(s + \frac{\lambda}{\beta}(1 - \exp(-\beta\eta))\right)\varphi' + \frac{N_T}{N_B}\theta'' = 0 \tag{29}$$

Equations (28)-(29) are supplemented by boundary conditions (18)-(19).

5. RESULTS AND DISCUSSIONS

The *bvp* method in Maple computer software is used to solve dimensionless ordinary differential equations (28)-(29) with boundary conditions (18)-(19). The results for the velocity profile are found analytically from expression (25), and as can be seen from expression (26), two analytical solutions are possible corresponding to the values of β. Similarity solutions exist when the mass suction parameter $s > 0$ and the parameter $\lambda < 0$ (shrinking sheet) (see Figs. 2 and 3).
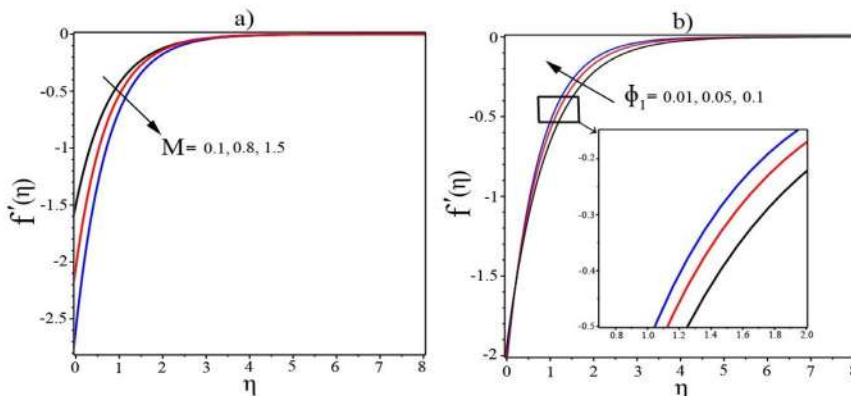
Figure 4. a) Effect of magnetic field on velocity profiles for $\phi_{tnf} = 0.13$; b) effect of volume fraction on velocity profiles for $M = 0.8$.
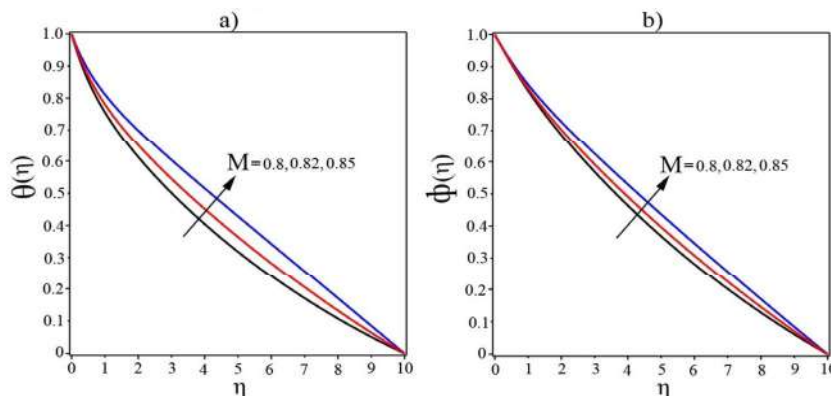
Figure 5. a) Effect of magnetic field on temperature for $\phi_{tnf} = 0.13$; b) effect of magnetic field on concentration profile for $\phi_{tnf} = 0.13$.

Figs. 4a and 4b show the influence of a magnetic field and a volume fraction on the velocity profile of a ternary hybrid nanofluid for shrinking case $\lambda = -2$ when the suction is presented as $s = 2$. Due to the very small difference between the solutions of the upper and lower branches for the velocity profile, Figs. 4a and 4b show graphs for the upper branch solutions. It can be seen from these figures that the boundary conditions at $\eta \to \infty$ (19) are achieved asymptotically. The calculations are performed out with an accuracy of 10^{-5} by setting $\eta_\infty = 10$ for the far field boundary conditions. The presence of a magnetic field produces a force known as the Lorentz force, which resists fluid flow. This force's magnitude is directly proportional to M value. As a result, increasing M increases the Lorentz force. As seen in Fig. 4a, the thickness of the boundary layer grows as M increases. From Fig. 4b, we observe that the fluid flow rate increases with an increase in the volume fraction of Cu-nanoparticles (ϕ_1).

The decrease in flow rate due to the increase in the magnetic field M allows the nanoparticles to conduct more heat, and hence an increase in temperature is observed as shown in Fig. 5a. Due to the effect of thermophoresis, an increase in the temperature profile also causes an increase in the concentration profile, as seen in Fig. 5b.

Figs. 6a and 6b show the effect of volume fraction on temperature and concentration profiles. As a result, with an increase in the volume fraction of Cu nanoparticles, new possibilities for increasing thermal conductivity appear, as shown in Fig. 6a. In addition, with an increase in the volume fraction of Cu nanoparticles, the concentration profile of the nanofluid increases (see Fig. 6b). This effect has applications in medicine when it is necessary to heat up soft tissues with the help of hybrid ferrofluids in the treatment of cancer. The results shown in Figs. 4-6 are in good agreement with the conclusions of the paper [23].
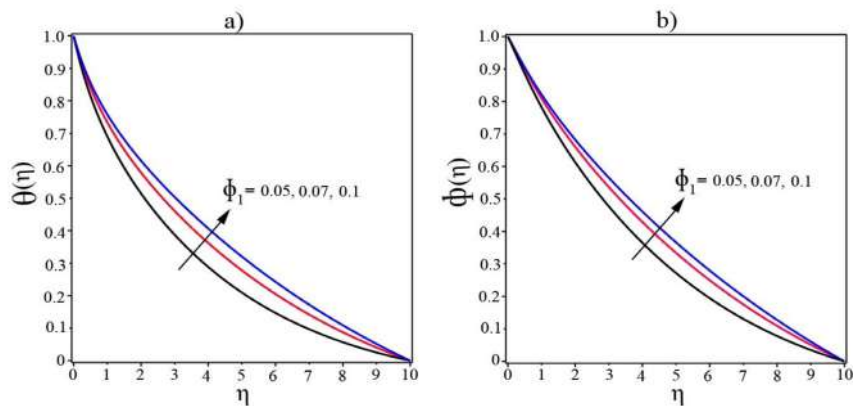
Figure 6. a) Effect of volume fraction ϕ_1 on temperature profile for $M = 0.8$; b) effect of volume fraction ϕ_1 on concentration profile for $M = 0.8$.

Fig. 7a and Fig. 7b show the temperature and concentration profiles for various N_T values. As shown in Fig. 7a, any small increase in the thermophoresis force (N_T) effectively increases the temperature profile. Due to the dependency of the concentration on the temperature field, we observe that higher thermophoresis parameters increase the concentration profile sharply (see Fig. 7b).

Adding more nanoparticles to the base fluid changed the behavior of the temperature and concentration profiles, as shown in Figs. 8a and 8b. The Brownian motion of nanoparticles plays a significant role in the distribution of heat, which is noticeable in the graph in Fig. 8a, where we observe an increase in the temperature profile with N_B. The concentration profile decreases as the Brownian motion parameter N_B increases, as shown in Fig. 8b.
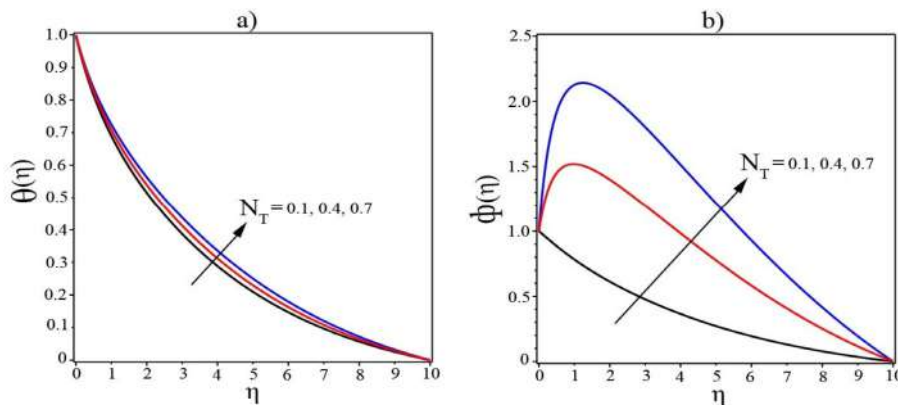

Figure 7. a) Temperature profiles for different values of N_T; b) concentration profiles for different values of N_T.
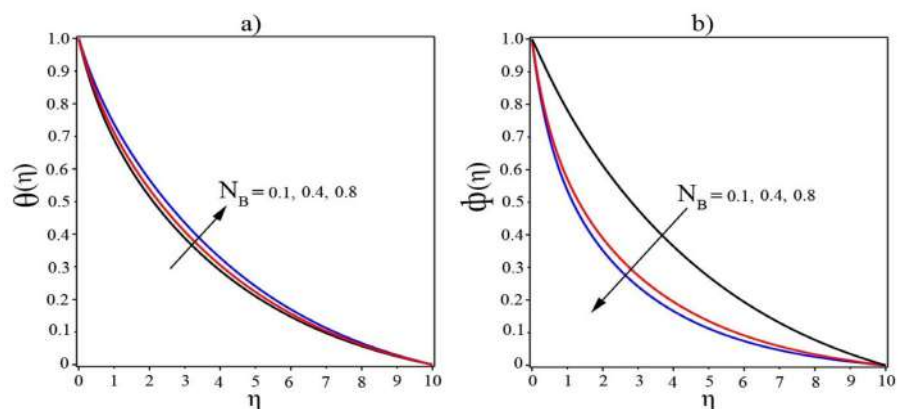

Figure 8. a) Temperature profiles for different values of N_B; b) concentration profiles for different values of N_B.

Figs. 9a and 9b show that both temperature and concentration profiles decrease with increasing Le. For analysis, we chose small values of Le, which correspond to the slightly viscous base fluid. The results shown in Figs. 7-9 are in good agreement with the conclusions of the paper [30].
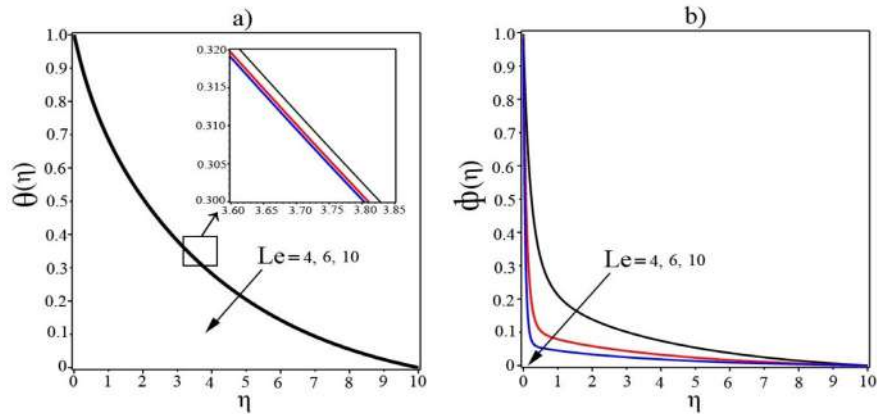
Figure 9. a) Effect of Le number on temperature distribution; b) effect of Le number on concentration distribution.

Fig. 10a depicts the variation of the skin friction coefficient Sr with the stretching/shrinking parameter λ for several values of the suction parameter s. When the shrinking parameter is changed from -2.046 to -6.090, the value of the suction parameter increases from $s = 2$ to $s = 4$. The double solution regions also expand with an increase in the suction parameter s at fixed values parameters of magnetic field $M = 0.8$ and volume fraction $\phi_{tnf} = 0.13$. Increasing the magnetic field parameter increases the coefficient of skin friction Sr, as shown in Fig. 10b. However, with an increase in ϕ_1, the coefficient of surface friction Sr decreases because thermal conductivity increases at a higher concentration of nanoparticles. Due to the fact that thermal conductivity is enhanced by increasing the concentration of copper particles, the Nusselt number (heat transfer rate) decreases (see Fig. 11a). As the magnetic field M increases, the rate of heat transfer and concentration decreases, but the rate of concentration increases with increasing ϕ_1, as shown in Fig. 11b.
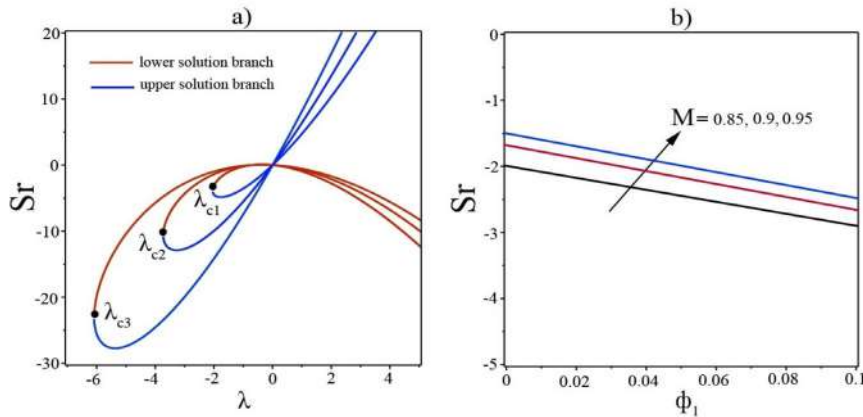

Figure 10. a) Variation of Sr as a function of λ for several values of s ($s = 2, \lambda_{c1} = -2.046$, $s = 3, \lambda_{c2} = -3.731$, $s = 4, \lambda_{c3} = -6.090$) for $\phi_{tnf} = 0.13$; b) effect of magnetic field and volume fraction on skin friction coefficient Sr.
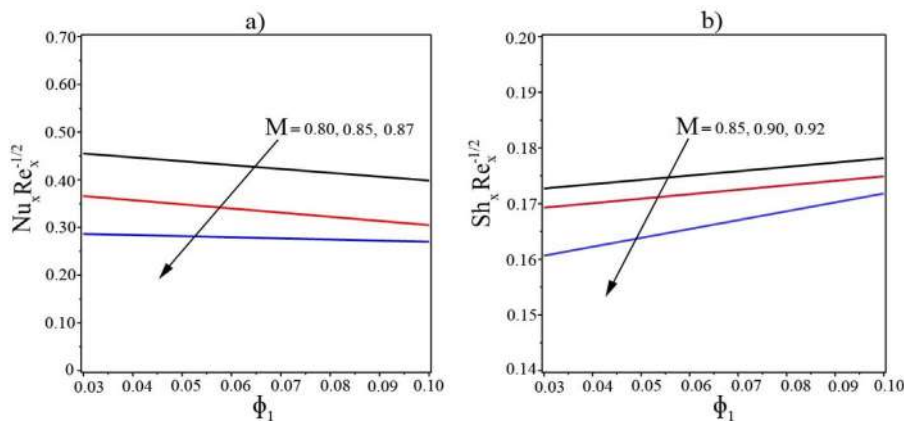

Figure 11. a) The influence of the magnetic field and volume fraction ϕ_1 on the local Nusselt number; b) the influence of the magnetic field and volume fraction ϕ_1 on the local Sherwood number.

Fig. 12a displayed the impact of Prandtl number Pr on the rate of heat transfer. An increase in the Prandtl number is associated with a decrease in the thermal conductivity of the base fluid k_f, which leads to an increase in heat transfer. Figure 12b depicts the influences of Nu_x as a function of M for various Nr. This graphic shows that Nu_x decreases as the examined two parameters (M and Nr) increase.

The change in the local heat and concentration transfer rates depending on the parameter N_T is shown in Figs. 13 and 14.
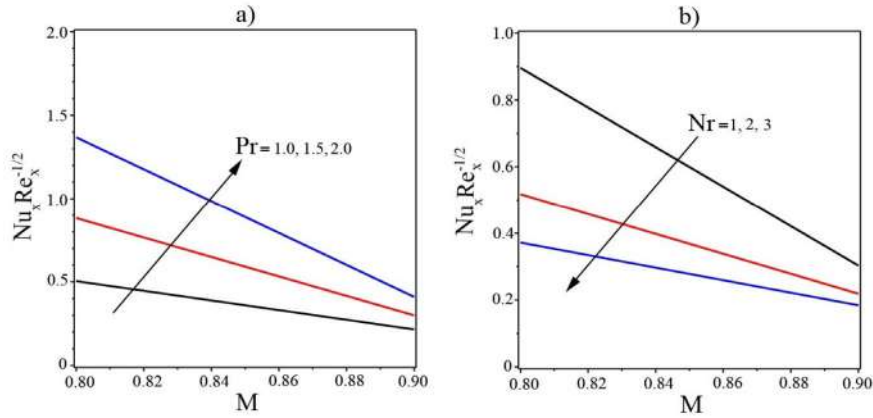

Figure 12. a) Effect of Prandtl number Pr and magnetic field on the local Nusselt number; b) effect of the radiation parameter Nr and magnetic field on the local Nusselt number.
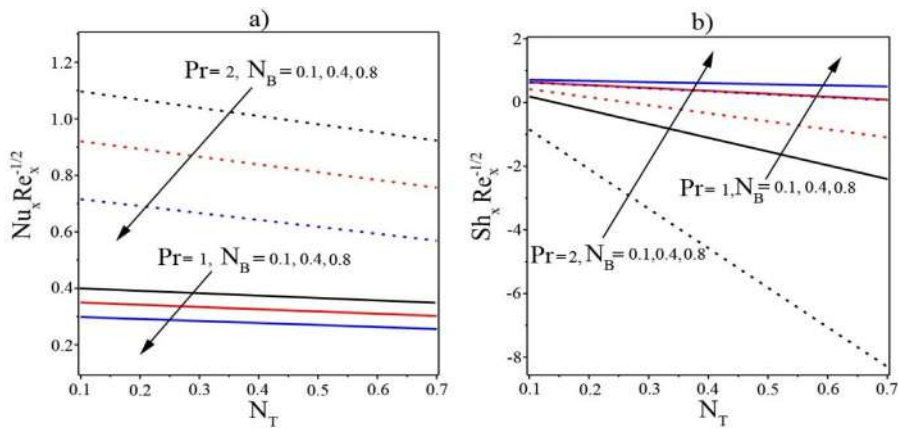

Figure 13. a) Effects of N_B and Pr numbers are seen on heat transfer rates; b) effects of N_B and Pr numbers are seen on dimensionless concentration rates.
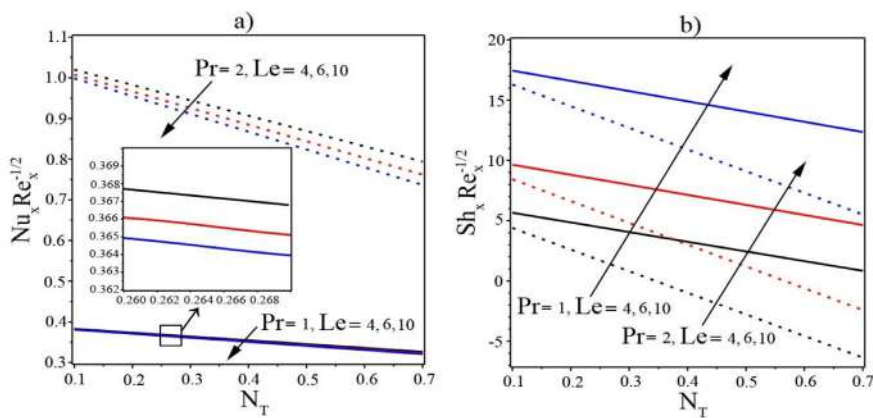

Figure 14. a) Effects of Le and Pr numbers are seen on heat transfer rates; b) effects of Le and Pr numbers are seen on dimensionless concentration rates.

Graphs in Fig. 13 show the effect of the N_B parameters and Pr Prandtl number on the local heat and concentration transfer rate for a fixed Le number. As can be seen from Fig. 13, the dimensionless heat transfer rate

decreases with increasing parameters N_B and N_T but increases with increasing Pr. The local Sherwood number Sh_x, on the other hand, increases as the Brownian motion parameter N_B increases but decreases as the Prandtl number increases. However, with an increase in the Le number, a decrease in the local heat transfer rates was observed. As shown in Fig. 14a, the change in local heat transfer rates increases with an increase in the Prandtl number. In contrast, the local Sherwood number increases with the Lewis parameter Le, but decreases with the Pr number, as shown in Fig. 14b. These results are in good agreement with the conclusions of the papers[24],[30].

6. CONCLUSIONS

An analysis was made of the diffusion characteristics of heat and nanoparticles in a ternary hybrid ferrofluid flow over a linearly stretching/shrinking porous sheet under conditions of mass transpiration and radiation heating. Using the similarity transformation, a system of nonlinearly coupled ODEs was obtained, which was numerically solved in the Maple software application using the *bvp* technique. Numerical results are interpreted using graphs. We have found the boundaries of the existence of unique and double solutions depending on the magnitude of the magnetic field for the shrinking case $(\lambda < 0)$. The main research results are:

• An increase in the magnetic field resists the flow of the trihybrid ferrofluid, while an increase in the volume fraction of nanoparticles increases the momentum of the flow.

• The skin friction coefficient increases with an increase in the suction rate $s > 0$ and the magnitude of the Lorentz force.

• The rates of heat and mass transfer decrease as the Lorentz force increases.

• The local Nusselt number (rate of heat transfer) decreases when the values of the parameters Pr, Le, N_B, Nr and N_T are increased.

• The local Sherwood number (rate of mass transfer) increases as the Brownian motion parameter increases and decreases as the thermophoresis parameter increases.

The results obtained can be generalized to other types of ternary hybrid nanofluids that are used in various practical problems.

ORCID IDs
Michael I. Kopp, https://orcid.org/0000-0001-7457-3272, **Volodymyr V. Yanovsky,** https://orcid.org/0000-0003-0461-749X
Thippeswamy Anusha, https://orcid.org/0000-0003-0950-6481; **Ulavathi S. Mahabaleshwar,** https://orcid.org/0000-0003-1380-6057

REFERENCES
[1] J. C. Maxwell, *A Treatise on Electricity and Magnetism* (Clarendon, Oxford, 1873)
[2] S. Choi, Enhancing thermal conductivity of fluids with nanoparticles, in: *Development and applications of Non-Newtonian flows*, edited by D.A. Signier and H.P. Wang, Vol. 66, (ASME, New York, 1995) pp. 99-105.
[3] B.C. Sakiadis, "Boundary layer behaviour on continuous solid surfaces: I. boundary layer equations for two-dimensional and axisymmetric flow", AIChE J. **7**, 26-28 (1961). https://doi.org/10.1002/aic.690070108
[4] B.C. Sakiadis, "Boundary layer behaviour on continuous solid surfaces: II. the boundary layer on a continuous flat surface", AIChE J. **7**, 221-225 (1961), https://doi.org/10.1002/aic.690070211
[5] L.J. Crane, "Flow past a Stretching Plate", Z. Angrew. Math. Phys. **21**, 645-647 (1970). https://doi.org/10.1007/BF01587695
[6] E.H. Aly, and I. Pop, "MHD flow and heat transfer near stagnation point over a stretching/shrinking surface with partial slip and viscous dissipation: Hybrid nanofluid versus nanofluid", Powder Technol. **367**, 192-205 (2020). https://doi.org/10.1016/j.powtec.2020.03.030
[7] U. Khan, A. Shafiq, A. Zaib, and D. Baleanu, "Hybrid nanofluid on mixed convective radiative flow from an irregular variably thick moving surface with convex and concave effects", Case stud. Therm. Eng. **21**, 100660 (2020). https://doi.org/10.1016/j.csite.2020.100660
[8] A. Jamaludin, K. Naganthran, R. Nazar, and I. Pop, "MHD mixed convection stagnation-point flow of Cu-Al2O3/water hybrid nanofluid over a permeable stretching/shrinking surface with heat source/sink", Euro. J. Mech. B/Fluids, **84**, 71-80 (2020). https://doi.org/10.1016/j.euromechflu.2020.05.017
[9] U.S. Mahabaleshwar, A.B. Vishalakshi, and H.I. Andersson, "Hybrid nanofluid flow past a stretching/shrinking sheet with thermal radiation and mass transpiration", Chinese Jour. Phys. **75**, 152-168 (2022). https://doi.org/10.1016/J.CJPH.2021.12.014
[10] T. Anush, U.S. Mahabaleshwar, and Y. Sheikhnejad, "An MHD of Nanofluid Flow Over a Porous Stretching/Shrinking Plate with Mass Transpiration and Brinkman Ratio", Transp. Porous Med. **142**, 333-352 (2021). https://doi.org/10.1007/s11242-021-01695-y
[11] K.E. Aslani, U.S. Mahabaleshwar, J. Singh, I.E. Sarris, "Combined effect of radiation and inclined MHD flow of a micro polar fluid over a porous stretching/shrinking sheet with mass transpiration", Int. J. Appl. Comput. Math. **7**, 1-21 (2021). https://doi.org/10.1007/s40819-021-00987-7
[12] U.S. Mahabaleshwar, K.N. Sneha, and H.N. Haung, "An effect of MHD and radiation on CNTs-water based nanofluids due to a stretching sheet in a Newtonian fluid", Case Stud. Therm. Eng. **28**, 101462 (2021). https: //doi.org/10.1016/j.csite.2021.101462
[13] R.E. Rosensweig, *Ferrohydrodynamics*, (Cambridge University Press, Cambridge, 1985)
[14] Y.M. Chu, S. Bilal, and M.R. Hajizadeh, "Hybrid ferrofluid along with MWCNT for augmentation of thermal behavior of fluid during natural convection in a cavity", Math. Methods Appl. Sci. **2020**, 1-12 (2020). https://doi.org/10.1002/mma.6937
[15] K.A. Kumar, N. Sandeep, V. Sugunamma, and I.L. Animasaun, "Effect of irregular heat source/sink on the radiative thin film flow of MHD hybrid ferrofluid", J. Therm. Anal. Calorim. **139**, 2145-2153 (2020). https://doi.org/10.1007/s10973-019-08628-4

[16] I. Tlili, M.T. Mustafa, K.A. Kumar, and N. Sandeep, "Effect of asymmetrical heat rise/fall on the film flow of magnetohydrodynamic hybrid ferrofluid", Sci. Rep. **10**, 6677 (2020). https://doi.org/10.1038/s41598-020-63708-y

[17] N.S. Anuar, N. Bachok, and I. Pop, "Influence of MHD Hybrid Ferrofluid Flow on Exponentially Stretching/Shrinking Surface with Heat Source/Sink under Stagnation Point Region", Mathematics, **9**, 2932 (2021). https://doi.org/10.3390/math9222932

[18] L.A. Lund, Z. Omar, J. Raza, and I. Khan, "Magnetohydrodynamic flow of Cu-Fe3O4/H2O hybrid nanofluid with effect of viscous dissipation: Dual similarity solutions", J. Therm. Anal. Calorim. **143**, 915-927 (2021). https://doi.org/10.1007/s10973-020-09602-1

[19] L.S. Sundar, K.V.V.C. Mouli, Z. Said, and A.C.M. Sousa, "Heat transfer and second law analysis of ethylene glycol-based ternary hybrid nanofluid under laminar flow", J. Therm. Sci. Eng Appl. **13**, 1-15 (2021). https://doi.org/10.1115/1.4050228

[20] U. Khan, and Z. Mahmood, "MHD Stagnation Point Flow of Ternary Hybrid Nanofluid Flow over a Stretching/Shrinking Cylinder with Suction and Ohmic Heating", Preprint, (2022). https://www.authorea.com/doi/full/10.22541/au.164873383.38887373

[21] G.K. Ramesh, J.K. Madhukesh, S.A. Shehzad, and A. Rauf, "Ternary nanofluid with heat source/sink and porous medium effects in stretchable convergent/divergent channel", Proc. Inst. Mech. Eng. E: J. Process Mech. Eng. **2022**, 1-10 (2022). https://doi.org/10.1177/09544089221081344

[22] I.L. Animasaun, S.J. Yook, T. Muhammad, and A. Mathew, "Dynamics of ternary-hybrid nanofluid subject to magnetic flux density and heat source or sink on a convectively heated surface", Surf. Interfaces **28**, 101654 (2022). https://doi.org/10.1016/j.surfin.2021.101654

[23] S. Manjunatha, V. Puneeth, B.J. Gireesha, and A.J. Chamkha, "Theoretical Study of Convective Heat Transfer in Ternary Nanofluid Flowing past a Stretching Sheet." J. Appl. Comput. Mech. **8**, 1279-1286 (2022). https://doi.org/10.22055/JACM.2021.37698.3067

[24] N.L. Aleng, N. Bachok, and N.M. Arifin, "Flow and Heat Transfer of a Nanofluid over an Exponentially Shrinking Sheet", Indian J. Sci. Technol. **8**, 1-6 (2015). https://doi.org/10.17485/ijst/2015/v8i31/87246

[25] J. Raza, A.M. Rohni, Z. Omar, and M. Awais, "Rheology of the Cu-H2O nanofluid in porous channel with heat transfer: Multiple solutions" Phys. E: Low-Dimens. Syst. Nanostructures, **86**, 248-252 (2017). https://doi.org/10.1016/j.physe.2016.10.038

[26] B. Takabi, and S. Salehi, "Augmentation of the heat transfer performance of a sinusoidal corrugated enclosure by employing hybrid nanofluid." Adv. Mech. Eng. **6,** 147059 (2014). https://doi.org/10.1155/2014/147059

[27] R.S.R. Gorla, S. Siddiqa, M.A. Mansour, A.M. Rashad, and T. Salah, "Heat source/sink effects on a hybrid nanofluid-filled porous cavity", J. Thermophys. Heat Transf. **31**, 847-857 (2017). https://doi.org/10.2514/1.T5085

[28] E. Magyari, and A.J. Chamkha, "Exact analytical results for the thermosolutal mhd marangoni boundary layers", Int. J. Therm. Sci. **47**, 848-857 (2008). https://doi.org/10.1016/j.ijthermalsci.2007.07.004

[29] P.G. Siddheshwar, and U.S. Mahabaleswar, "Effects of radiation and heat source on MHD flow of a viscoelastic liquid and heat transfer over a stretching sheet", Int. J. Non-Linear Mech. **40**, 807-820 (2005). https://doi.org/10.1016/j.ijnonlinmec.2004.04.006

[30] A. Alam, D.N.K. Marwat, and A. Ali, "Flow of nano-fluid over a sheet of variable thickness with non-uniform stretching (shrinking) and porous velocities", Adv. Mech. Eng. **13**, 1-16 (2021). https://doi.org/10.1177/16878140211012913

МГД ТЕЧІЯ І ТЕПЛОПЕРЕДАЧА ПОТРІЙНОЇ ГІБРИДНОЇ ФЕРОРІДИНИ НАД ПОРИСТИМ ЛИСТОМ, ЩО РОЗТЯГУЄТЬСЯ/СТИСКАЄТЬСЯ, З ЕФЕКТАМИ БРОУНІВСЬКОЇ ДИФУЗІЇ ТА ТЕРМОФОРЕЗУ

Михайло Й. Копп[a], Володимир В. Яновський[a,b], Тіпсвамі Ануша[c], Улаваті С. Махабалешвар[c]
[a]Інститут монокристалів, Національна Академія Наук України
пр. Науки 60, 61001 Харків, Україна
[b]Харківський національний університет імені В.Н. Каразіна
майдан Свободи, 4, 61022, Харків, Україна
[c]Факультет математики, Шівангангтрі, Університет Давангере, Давангере, Індія 577 007

В даній роботі досліджується магнітогідродинамічна (МГД) течія потрійної гібридної ферорідини над пористим листом, що розтягується/стискується, в присутності випромінювання і масової транспірації. Потрійна гібридна нанорідина утворюється шляхом суспендування трьох типів наночастинок для покращення теплопередачі. Наночастинки міді (Cu), оксиду заліза (Fe_3O_4) та фериту кобальту $(CoFe_2O_4)$ суспендовані у воді та утворюють комбінацію $Cu - Fe_3O_4 - CoFe_2O_4 - H_2O$. Броунівський рух та термофорез інтегровані в модель потрійної гібридної ферорідини. Перетворення подібності конвертують основні диференціальні рівняння в приватних похідних у звичайні диференціальні рівняння. Метод розв'язання крайової задачі використовується в програмному забезпеченні Maple для чисельного розв'язання перетворених рівнянь. Результати обчислень для відповідних параметрів, таких як профіль швидкості, температурний профіль, коефіцієнт поверхневого тертя, локальні числа Нуссельта та Шервуда, наочно показані і докладно пояснені.
Ключові слова: *потрійна гібридна ферорідина; розтягнення/стиск; тепло- та масообмін; масова транспірація; магнітне поле*